Aerosol Science and Technology

ISSN: (Print) (Online) Journal homepage: www.tandfonline.com/journals/uast20

Reactive oxygen species, environmentally persistent free radicals, and oxidative potential of outdoor and indoor particulate matter in Wintertime Fairbanks, Alaska

Sukriti Kapur, Kasey C. Edwards, Ting Fang, Meredith Schervish, Pascale S. J. Lakey, Yuhan Yang, Ellis S. Robinson, Peter F. DeCarlo, William R. Simpson, Rodney J. Weber & Manabu Shiraiwa

To cite this article: Sukriti Kapur, Kasey C. Edwards, Ting Fang, Meredith Schervish, Pascale S. J. Lakey, Yuhan Yang, Ellis S. Robinson, Peter F. DeCarlo, William R. Simpson, Rodney J. Weber & Manabu Shiraiwa (13 Dec 2024): Reactive oxygen species, environmentally persistent free radicals, and oxidative potential of outdoor and indoor particulate matter in Wintertime Fairbanks, Alaska, Aerosol Science and Technology, DOI: 10.1080/02786826.2024.2433656

To link to this article: https://doi.org/10.1080/02786826.2024.2433656

AEROSOL SCIENCE AND TECHNOLOGY
https://doi.org/10.1080/02786826.2024.2433656

Reactive oxygen species, environmentally persistent free radicals, and oxidative potential of outdoor and indoor particulate matter in Wintertime Fairbanks, Alaska

Sukriti Kapur[a], Kasey C. Edwards[a], Ting Fang[a,b], Meredith Schervish[a], Pascale S. J. Lakey[a], Yuhan Yang[c], Ellis S. Robinson[d], Peter F. DeCarlo[d], William R. Simpson[e], Rodney J. Weber[c], and Manabu Shiraiwa[a]

[a]Department of Chemistry, University of California, Irvine, California, USA; [b]Sustainable Energy and Environment Thrust, The Hong Kong University of Science and Technology (Guangzhou), Guangzhou, China; [c]School of Earth and Atmospheric Sciences, Georgia Institute of Technology, Atlanta, Georgia, USA; [d]Department of Environmental Health and Engineering, Johns Hopkins University, Baltimore, Maryland, USA; [e]Department of Chemistry and Biochemistry, University of Alaska, Fairbanks, Alaska, USA

ABSTRACT

Sub-arctic cities can face episodes of high air pollution during wintertime that can lead to human exposure to high concentrations of particulate matter. During the ALPACA campaign in Fairbanks, Alaska in January – February 2022, we conducted sampling of outdoor fine particulate matter ($PM_{2.5}$) using a high-volume sampler and indoor PM using a size-segregated cascade impactor in a house during activities including cooking and residential heating using a pellet stove. We aimed to characterize health-related properties of outdoor and indoor PM by measuring environmentally persistent free radicals (EPFRs) and reactive oxygen species (ROS) using electron paramagnetic resonance (EPR) spectroscopy. We also quantified PM oxidative potential (OP) using the dithiothreitol (OP-DTT) and OH (OP-OH) assays. We found that outdoor PM generates •OH (67%) and carbon-centered radicals (33%), while indoor PM predominantly forms •OH (93%) in water. Indoor activities of pellet stove burning generated substantial amounts of EPFRs in submicron PM. Both indoor and outdoor ROS exhibit little correlations with OP-DTT. Outdoor •OH correlates well with water-soluble iron ($R^2 = 0.51$), indicating the role of Fenton(-like) reactions in generating •OH in the aqueous phase. Both OP-OH and the modeled OH production rate in lung lining fluid correlate strongly with EPFRs, indicating that EPFRs are redox active to generate •OH. We also observe that EPFRs show a weak correlation with measured •OH formation in water but with a much stronger correlation with measured •OH in surrogate lung fluid, emphasizing the importance of lung antioxidants for redox cycling of EPFRs in the generation of •OH.

GRAPHICAL ABSTRACT

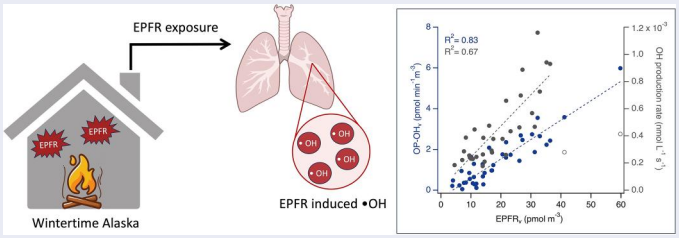

ARTICLE HISTORY
Received 18 July 2024
Accepted 8 November 2024

EDITOR
Andrea Ferro

Introduction

Wintertime air pollution poses a significant concern in the Arctic and sub-Arctic regions. The pollution is mainly attributed to local emissions that are poorly dispersed due to severe temperature inversions associated with a very shallow boundary layer (Marelle et al. 2018; Thomas et al. 2019). Fairbanks, Alaska is one such city having poor air quality in winter. With a

CONTACT Manabu Shiraiwa m.shiraiwa@uci.edu Department of Chemistry, University of California, 1102 Natural Sciences II, Irvine, CA 92697-2025, USA.

Supplemental data for this article can be accessed online at https://doi.org/10.1080/02786826.2024.2433656.

population of ~32,000 within city limits, Fairbanks has a subarctic climate, with short warm summers and very cold winters with temperature as low as −40 °C with frequent and strong surface-based inversions (Fochesatto et al. 2015; Wendler and Shulski 2009; Cesler-Maloney et al. 2022). Fairbanks is located within a three-side basin and the Alaska range on the fourth side, and hence the air within the city is relatively stagnant with low wind conditions, preventing pollutant dispersion (Bowling 1979). In addition, there is very limited sunlight in winter in Fairbanks, resulting in very low photochemistry (Joyce, Von Glasow, and Simpson 2014). Concentrations of $PM_{2.5}$ (particulate matter with particle diameter less than 2.5 μm) in Fairbanks often exceed the 24-h National Ambient Air Quality Standards (NAAQS) of 35 μg m^{-3}; hence, the U.S. Environmental Protection Agency has identified Fairbanks as an air quality nonattainment zone. Average $PM_{2.5}$ concentrations were reported to be as high as 70 μg m^{-3} in the winter 2020 (Cesler-Maloney et al. 2022). Most people in the United States spend ~90% of their time indoors (United States Environmental Protection Agency n.d.) and this number is even higher under extreme winter climates in Fairbanks. Indoor heating with residential wood burning can lead to increased levels of indoor pollutants that may cause adverse health impacts (Vicente et al. 2020; Oeder et al. 2012) and is reported to be the largest source of outdoor $PM_{2.5}$ in winter months in Fairbanks (Ward et al. 2012; Kotchenruther 2016).

Atmospheric PM generated from incomplete combustion can contain significant amounts of stable radicals, known as environmentally persistent free radicals (EPFRs) (Jia et al. 2020; Chen et al. 2020; Dellinger et al. 2000). These radicals are resonance stabilized with a chemical structure similar to semiquinone radicals, leading to a long lifetime from minutes to no decay (Dellinger et al. 2007; Gehling and Dellinger 2013; Khachatryan et al. 2011). EPFRs are often emitted by vehicle tailpipe and biomass burning (Hwang et al. 2021; Fang et al. 2023), while they can also be formed secondarily by multiphase oxidation of polycyclic aromatic hydrocarbons (PAHs) (Tong et al. 2018; Borrowman et al. 2016; Edwards et al. 2022). EPFRs are redox active and catalytically form reactive oxygen species (ROS) in the aqueous phase (Khachatryan et al. 2011; Khachatryan and Dellinger 2011). ROS are typically defined to include hydroxyl radical (•OH), superoxide ($•O_2^-$), hydroperoxyl radical ($•HO_2$), hydrogen peroxide (H_2O_2), and organic radicals (Pöschl and Shiraiwa 2015). They play an important role in inducing oxidative stress and adverse health effects of $PM_{2.5}$ by causing oxidative damage to proteins, lipid membranes, and DNA (Finkel and Holbrook 2000; Sies, Berndt, and Jones 2017; Shiraiwa et al. 2017). In addition to redox reactions of EPFRs, ROS can be generated by other $PM_{2.5}$ components *via* Fenton-like reactions of transition metals, redox cycling of humic-like substances, and decomposition of organic hydroperoxides and subsequent aqueous reactions (Charrier and Anastasio 2015; Tong et al. 2018; Vidrio, Jung, and Anastasio 2008; Win et al. 2018; Wei et al. 2021a; Wei et al. 2021b).

PM oxidative potential (OP) represents the redox activity of PM, serving as an indication for the depletion of antioxidants or generation of ROS (Cho et al. 2005; Fang et al. 2016). OP is most commonly characterized by the dithiothreitol (DTT) assay, which is an analytical method that is reproducible, cost effective, and easy to perform. This assay is sensitive to key components including quinones, transition metals and humic-like substances (HULIS) (Charrier and Anastasio 2012; Fang et al. 2015; Gao et al. 2017; Jiang et al. 2019; Kumagai et al. 2002; Verma et al. 2015). The OP-OH assay measures the formation rate of •OH in surrogate lung fluid containing the major lung antioxidants (Shen et al. 2022). While these assays are widely used to evaluate the toxicity of atmospheric PM (Salana et al. 2024; Daellenbach et al. 2020), the underlying relationship among OP, EPFRs, ROS formation, and overall PM toxicity remain unelucidated (Fang et al. 2019; Xiong et al. 2017).

EPFRs, ROS formation and oxidative potential of PM in cold and dark conditions and indoor environments are not well characterized. This knowledge gap is particularly stark for cities like Fairbanks, which experience extreme meteorological conditions with high pollution episodes. To address this understudied topic, we conducted outdoor and indoor PM sampling during the Alaskan Layered Pollution And Chemical Analysis (ALPACA) field campaign in Fairbanks, AK during January-February 2022 (Simpson et al. 2024). A Hi-Volume $PM_{2.5}$ sampler was used outdoors, while size-segregated indoor sampling was conducted using a cascade impactor during indoor activities of cooking or pellet stove heating. The collected PM samples were analyzed for EPFRs, ROS and OP. Recent studies from the same field campaign have reported the oxidative potential of outdoor and indoor PM characterized by the DTT assay (Yang et al. 2024b) and contrasted outdoor OP measured with the DTT and OH production assays and $PM_{2.5}$ mass concentration for Fairbanks and other urban regions (Yang et al. 2024a). Edwards et al. (2024) reported outdoor

sources and concentrations of EPFRs. The objective of this study is to further elucidate the health-relevant properties of PM and to evaluate PM exposure in cold and dark environments by examining relations between EPFRs, ROS, and OP for outdoor and indoor PM.

Materials and methods

PM collection

We conducted indoor and outdoor PM sampling at a rented house (64.850°N, 147.676°W) in the Shannon Park neighborhood, North-East Fairbanks, Alaska. This location was selected due to its proximity to an urban and residential pollution impacted site in the Hamilton Acres neighborhood; Alaska Department of Environmental Conservation A-Street site (Simpson et al. 2024; Robinson et al. 2023).

For outdoor sampling, a Hi-Vol sampler was used (Tisch Environmental, flow rate 1.13 m^3 min^{-1}) to collect ambient $PM_{2.5}$ onto prebaked 8″ × 10″ micro quartz filters. The sampler was placed in the outdoor back porch and $PM_{2.5}$ samples were collected for 23.5 h daily from 01/16/2022 to 02/25/2022. Field blanks were collected once a week at the same location by loading the filters to the Hi-Vol sampler without turning on the pump for 30 s. After collection, filters were wrapped in prebaked aluminum foil and immediately stored in a freezer (−18 °C). Portions of the filters were cut using a circular punch (diameter of 2.54 cm) and analyzed for EPFR, ROS and OP-DTT.

For indoor sampling, a Micro-Orifice Uniform Deposition Impactor (MOUDI, Model 100NR) was used to collect size-segregated indoor PM on Teflon filters (Millipore Omnipore Membrane Filter, PTFE, 0.2 µm pore size, JFWP04700). The MOUDI was operated at 30 L min^{-1} with the selected stages with 50% cutoff aerodynamic diameters of 18, 10, 1, 0.18, 0.056 µm, in addition to a blank filter. The MOUDI was placed in the living room, near a pellet-burning fireplace insert stove (Harman P35i) during indoor activities including oil-based cooking, chicken tender frying, pellet-burning, or a mix of both (see details in SI). At all other times the house was unoccupied. All doors were closed, and household occupation was kept minimum. The house was depressurized by 50 Pa for a blower door test, and leakage into the house was estimated to be 0.12 air changes per hour (Simpson et al. 2024; Yang et al. 2024b). Background sampling was conducted for 6 h on days without indoor activities. Sixteen sets of filter samples, including background, were collected. After the collection, all filters were stored in petri dishes and immediately stored in a freezer (−18 °C). EPFRs, ROS formation, and OP-DTT measurements were performed on these filter samples, following procedures in our previous study (Hwang et al. 2021). Details on sample stability and analysis times and quality assurance/control are described in the SI.

Environmentally persistent free radicals (EPFRs)

One inch diameter circular punch from a quartz filter or the entire PTFE filter was inserted in a quartz tube (inner diameter of 9.17 mm), then loaded into the resonator of a continuous-wave electron paramagnetic resonance (CW-EPR) spectrometer (EMXplus, Bruker, Germany). The following EPR parameters were used for EPFR measurements: a microwave frequency of 9.65 GHz; a microwave power of 20 or 31.70 mW (microwave attenuation 8 or 10 dB); a modulation frequency of 100 kHz; a modulation amplitude of 3 G; a receiver gain of 40 dB; a time constant of 10.24 ms; and a magnetic field scan of 1623 G. The area of EPR spectrum was integrated using the Xenon software and converted to total number of spins based on a calibration using standard 4-hydroxy-2,2,6,6-tetramethylpiperidinyloxy (TEMPOL) solutions (Figure S2, R^2 = 0.99). Concentrations were reported as per-air volume ($EPFR_v$, in pmol m^{-3}) as a relevant metric for exposure and per-PM mass ($EPFR_m$, in pmol μg^{-1}) representative of an intrinsic health-relevant PM property.

Reactive oxygen species (ROS)

We measured ROS using EPR with a spin trapping technique. One inch diameter circular punch from the outdoor quartz filters or half the PTFE filter was extracted in 500 µL solution of 20 mM BMPO (5-tert-Butoxycarbonyl-5-methyl-1-pyrroline-N-oxide) in water. The extraction efficiency for PTFE filters is typically around 90%. For quartz filters, extraction efficiency cannot be determined due to filter disintegration in the solution, but the filters remained in the solution throughout the analysis, and we expect all constituents to interact with the reagents. BMPO is a spin trapping agent, reacting with radicals to form stable radical adducts that can be detected by EPR. The extract was vortexed for 7–9 min, concentrated 5–10 times by blowing under nitrogen gas for about 15 min and analyzed at 46 min from extraction. The EPR parameters used for ROS measurement were the same as those for EPFRs except a microwave

frequency of 9.87 GHz; a magnetic field scan of 150 G; a modulation amplitude of 1 G; and a time constant of 20.48 ms. Deconvolution and quantification of radicals was done using the spin-fit and spin-count software embedded in the Bruker Xenon Software. Concentrations were calculated and reported as ROS per-air volume (ROS_v, in pmol m^{-3}) and ROS per-PM mass (ROS_m, in pmol μg^{-1}).

Total dithiothreitol (OP-DTT) activity

Two circular punches from a quartz filter or the half PTFE filter were extracted in water by vortexing for 7–9 min. The extracts were incubated with potassium phosphate buffer and DTT (1 mM). The ratio of water: phosphate buffer: DTT was set to 7:2:1. Note that the filter was included in the extracts and our measurements represent the total DTT activity of PM including soluble and insoluble components. To quench DTT consumption, a small aliquot (50 μL) of the mixture was taken at specific time points and mixed with 0.5 mL 10% v/v. trichloroacetic acid. The solution was then mixed with 1 mL of Tris buffer (0.08 M with 4 mM EDTA (ethylenediaminetetraacetate), 0.250 mL of DTNB (0.2 mM, 5,5′-dithiobis (2-nitrobenzoic acid)) and diluted with 10 mL of water and filtered using a 0.22 µm pore syringe filter. The absorbance of the filtered solution was measured at 412 and 700 nm wavelength using the liquid waveguide capillary cell (path length = 100 cm; World Precision Instruments, Inc.) coupled with a UV-visible spectrophotometer (DH-MINI, Ocean Optics, Inc.) and multiwavelength light detector (FLAME-T-UV – vis-ES, Ocean Optics, Inc.). The DTT decay per time was reported as total DTT activity per-air volume ($OP\text{-}DTT_v$, in pmol min^{-1} m^{-3}) and DTT activity per-PM mass ($OP\text{-}DTT_m$, in pmol min^{-1} μg^{-1}).

Hydroxyl radical generation in surrogate lung fluid (OP-OH assay)

The high-volume filters were analyzed for OP by OH production in synthetic lung fluid assay (OP-OH) for $PM_{2.5}$ following the protocol described by Yu et al. (2021). A fraction from each filter was placed in a sterile polypropylene centrifuge vial (VWR International LLC, Suwanee, GA, USA). Due to the possible nonlinear response of OP endpoints with PM mass concentration (Shahpoury et al. 2022), the punched filter fraction and the volume of water used for extraction were determined based on the $PM_{2.5}$ mass loading on each filter to achieve a relatively constant sample concentration 25 µg mL^{-1} for OP-OH analysis in the reaction vial. Filters were extracted in deionized Milli-Q water (DI, Nanopure Infinity™ ultrapure water system; resistivity > 18 MΩ/cm) *via* 60 min sonication (Ultrasonic Cleanser, VWR International LLC, West Chester, PA, USA). PM extracts were not filtered, and the filter punch was left in the extracts throughout the OP analysis so insoluble species could be in contact with the reagents. The PM extract was mixed with surrogate lung fluid consisting of a mixture of 2.5 mM ascorbic acid, 1.25 mM reduced glutathione (GSH), and 1.25 mM uric acid, which was dissolved in phosphate-buffered saline (PBS, PH ∼7.4) along with potassium phosphate-buffered disodium terephthalate (TPT) (50 mM; pH ∼7.4). The mixing solution was incubated at 37 °C and shaken at a rotational frequency of 400 rpm. At selected time intervals (30, 60, 90 and 120 min), 2 mL of this reaction mixture were withdrawn and mixed with dimethyl sulfoxide (DMSO, 100 mM; 1 mL) to quench the reaction between ·OH and TPT. The reaction product of TPT and ·OH is 2-hydroxyterephthalic acid (2-OHTA), a fluorescent product that is measured at an excitation/emission wavelength of 310/427 nm by a Shimadzu Spectro fluorophotometer (RF-5301PC). The concentration of 2-OHTA was determined by calibrating with ten different concentrations (0–500 nM) of 2-OHTA standards, and the generation rate of ·OH was determined as the formation rate of 2-OHTA divided by a yield factor of 0.35 (Son et al. 2015). The OP of PM measured was blank-corrected and normalized by the air volume that passed through the extracted filter (volume-normalized, $OP\text{-}OH_v$) or the PM mass loading on the extracted filter (mass-normalized, $OP\text{-}OH_m$).

Elemental analysis

To measure the water-soluble elements collected on the filters, one circular filter punch was extracted in 5 mL of DI water *via* a 60-min sonification. The extracts were then filtered using a 0.45 µm PTFE syringe filter to obtain the water-soluble metals, which include all dissolved forms and colloidal particles with a diameter less than 0.45 µm. The filtered extract was acid- preserved with concentrated nitric acid (70%) to a final concentration of 2% (v/v) to keep the metals suspended in solution. To measure the total metal concentration, one 1.5 cm^2 filter punch from the Hi-Vol quartz filter was acid-digested using aqua regia (HNO_3+3HCl). The filter was incubated in the acid at 99 °C and shaken at a rotational frequency of 400 rpm using a ThermoMixer (Eppendorf North America,

Inc., Hauppauge, NY, USA) for 24 h. The acid-digested sample was then diluted in DI water to a final nitric acid concentration of 2% (v/v) and filtered through a 0.45 µm PTFE syringe filter (Yang, Gao, and Weber 2021). Both total and water-soluble elements were analyzed by inductively coupled plasma mass spectrometry (ICP-MS, Agilent 7500a series, Agilent Technologies, Inc., CA, USA) following the EPA method 6020 (United States Environmental Protection Agency 2014). Concentrations of magnesium, aluminum, potassium, manganese, iron, copper, zinc and lead are reported here.

OC/EC analysis and $PM_{2.5}$ mass

To determine the organic carbon (OC) and elemental carbon (EC) in $PM_{2.5}$ in Fairbanks, a 1.5 cm^2 filter punch was analyzed by a Sunset OC/EC analyzer (Sunset Laboratory Inc. OR, USA) using the National Institute for Occupational Safety and Health (NIOSH) 5040 analysis protocol (Birch and Cary 1996). Total carbon (TC) was calculated by summing OC and EC. Polycyclic aromatic hydrocarbons (PAHs), hydrocarbon-like organic aerosols (HOA), and biomass burning organic aerosols (BBOA) data were obtained from High-Resolution Time-of-Flight Aerosol Mass Spectrometer (HR-ToF-AMS, Aerodyne Research, Inc., USA) that measured PM_1 at the house site in Fairbanks (64.8502 N, −147.6755°E) with analysis into these OA factors using positive matrix factorization. Daily outdoor $PM_{2.5}$ mass concentrations (µg m^{-3}) were calculated by the summation of elemental carbon (EC) and AMS measured species (sulfate, nitrate, ammonium, organics, and chlorine) to the filter sampling times. The AMS measures non-refractory species only, leading to an underestimation of $PM_{2.5}$ mass. However, the difference between the calculated and observed $PM_{2.5}$ mass from a monitor 800 m WSW of the house site was 25% (Edwards et al. 2024). Indoor PM mass data was calculated by the mass differences of the filters before and after sampling.

Modeling ROS in epithelial lining fluid

Measured ambient concentrations of water-soluble iron and copper, $PM_{2.5}$, and EPFRs were used as inputs into the kinetic multi-layer model of surface and bulk chemistry in the epithelial lining fluid (KM-SUB-ELF) in order to predict the concentrations and production rates of ROS in the epithelial lining fluid upon inhalation and respiratory deposition of $PM_{2.5}$ (Lakey et al. 2016). This model has been applied in epidemiological studies and found to correlate with negative health outcomes including respiratory and cardiovascular diseases as well as COVID-19; thus, ROS levels in the lung have been shown to be an effective exposure metric (Stieb et al. 2021; Ripley et al. 2023). Ambient concentrations of input species are converted to concentrations in the ELF using an assumed breathing flow rate of 1.5 m^3 h^{-1} and deposition efficiency of 45%, as detailed in Lakey et al. (2016) and Fang et al. (2019). The model treats mass transport and over 50 chemical reactions involving antioxidants, redox-active compounds, and ROS. The treated chemistry includes reactions of ROS with antioxidants and surfactants, the formation of ROS from the redox cycling of Fe and Cu ions and quinones with ascorbate and oxygen, and the interconversion of ROS due to Fenton and Fenton-like chemistry. The rate coefficients used are the same as given in Lakey et al. (2016) and are assigned from literature values or have been previously determined by fitting experimental data. In this work, we assume that the chemical identity of EPFRs is semiquinone radicals, inputting EPFRs as semiquinone radicals with the same reactivity.

Results and discussion

Characterization of EPFRs, ROS, and OP

Figures 1a–c depicts results from EPR measurements of outdoor $PM_{2.5}$ samples. Figure 1a shows a typical EPR signal for EPFRs observed during the campaign. Our results show an average g-value of 2.0021 ± 0.0001 and a peak-to-peak distance of 6 ± 1 G, confirming the presence of EPFRs as similar to previous measurements (Hwang et al. 2021; Fang et al. 2023). Generally, a g-factor of <2.003 is indicative of a carbon-centered radical, 2.003–2.004 for carbon-centered free radicals adjacent to an oxygen atom and a value of >2.004 for oxygen-centered radicals (Dellinger et al. 2007; Chen et al. 2019; Ahmad et al. 2023). Figure 1b shows observed EPR spectra (black) for $PM_{2.5}$ extracts in water. Deconvolution of the spectra allows us to quantitively assess contributions from different radicals (Arangio et al. 2016). The simulated spectrum (green) shows contributions from different radicals, with dashed lines indicating the peaks for each type of radical species. The four and six peaks correspond to BMPO-OH (red) and BMPO-R (blue) adducts, indicating the formation of hydroxyl and carbon-centered radicals, respectively. The formation of •OH is also confirmed using the OH measurements with TPT in water (S1.4 and Figure S3). We did not observe the formation of superoxide and oxygen-centered organic

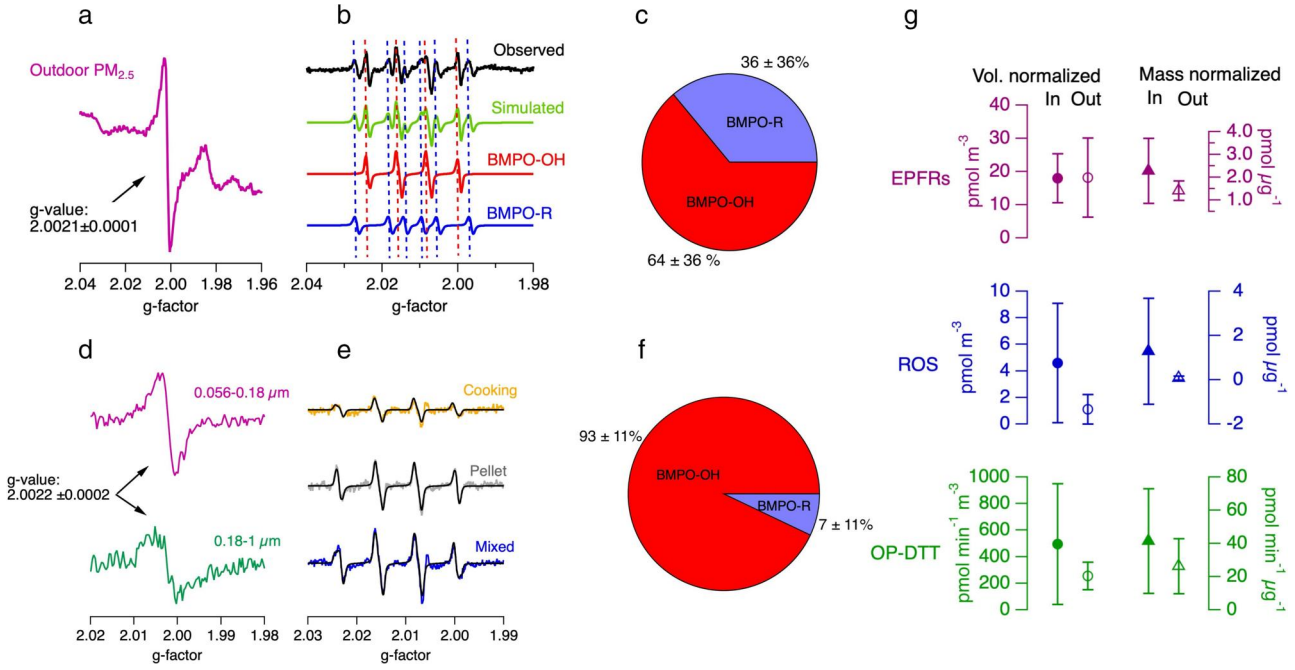

Figure 1. (a) Typical EPR spectrum of outdoor $PM_{2.5}$ in Fairbanks, showing the presence of EPFRs. (b) Observed (black) EPR spectrum of aqueous extracts of outdoor $PM_{2.5}$ and the simulated (green) spectrum by deconvolution into hydroxyl (•OH, red) and carbon-centered (•R, blue) radicals trapped by spin trapping agent BMPO. The dashed vertical lines represent different BMPO-radical adducts. (c) Average fractions of •OH and •R in aqueous extracts of outdoor $PM_{2.5}$. (d) Representative EPR spectra for size-segregated indoor sampling for EPFRs from pellet burning in particle diameter range of 0.056–0.18 μm and 0.18–1 μm. (e) Observed and simulated (black) EPR spectra for water extracts of indoor PM (particle diameter of 0.18–1 μm) during different activities. The generated radicals were trapped by BMPO. (f) Average fractions of •OH and •R in indoor PM. (g) Average air-volume normalized and PM-mass normalized concentrations of EPFRs and ROS and total OP-DTT activities of PM collected during indoor activities (solid markers) and outdoor sampling (open markers). Indoor PM is the sum of all MOUDI stages from 0.056 to 18 μm, while outdoor PM is for particle diameter less than ≤2.5 μm. Error bars represent one standard deviation (±1 SD) of the measurements.

radicals. Figure 1c shows the relative contribution of different radical adducts to the total radicals from ambient $PM_{2.5}$ averaged over the campaign, showing that •OH and carbon-centered radicals contribute 64% and 36% to total radicals, respectively. These results are consistent with previous measurements of ambient PM samples collected in urban cities in Mainz (Germany) (Arangio et al. 2016), Beijing (China) (Tong et al. 2021), and Irvine (USA) (Hwang et al. 2021) and in a remote forest in Hyytiälä (Finland) (Tong et al. 2021), which also observed dominant formation of •OH and carbon-centered radicals with minor contributions from superoxide and oxygen-centered organic radicals.

Figures 1d and e exhibit EPR spectra for EPFRs and ROS for indoor PM, respectively. Representative EPFR spectra are shown for PM with particle diameter of 0.056–0.18 μm and 0.18–1 μm collected during pellet burning activity. The observed g-value of ~2.0022 ± 0.0002 is similar to outdoor PM, indicating that indoor and outdoor EPFRs have a similar chemical identity. Figure 1e shows the observed and simulated spectra for spin trapped aqueous extracts of PM in the size range of 0.18–1 μm collected during cooking, pellet burning and mixed activities conducted in the house. All spectra show the presence of characteristic four peaks indicative of BMPO-OH, which was predominantly (~93%) observed for all indoor activities along with a small contribution (7%) from carbon-centered radical (•R) (Figure 1f).

Figure 1g depicts average concentrations of EPFRs, ROS and OP-DTT activities as normalized by air volume and PM mass. Indoor $EPFR_v$ is 18.0 ± 7.4 pmol m^{-3}, while outdoor $EPFR_v$ is 18.2 ± 11.9 pmol m^{-3}. When compared to EPFR concentrations previously reported from other locations, the outdoor $EPFR_v$ in Fairbanks is up to 11 times higher than U.S. urban cities such as Irvine and Denver (Hwang et al. 2021; Runberg et al. 2020), but much lower than highly polluted urban cities in China such as Linfen and Beijing (Chen et al. 2020; Yang et al. 2017). $EPFR_m$ for outdoors is 1.41 ± 0.42 pmol μg^{-1}, while for indoors it is 2.28 ± 1.42 pmol μg^{-1}. These values are comparable to previously reported values in Mainz, Germany (Arangio et al. 2016) and in US urban cities (Squadrito et al. 2001). Outdoor $EPFR_v$ shows a strong correlation with $PM_{2.5}$ mass concentration (Figure S5A).

Average indoor ROS_v concentration during the pellet, cooking and mixed activities is 4.6 ± 4.5 pmol m^{-3}, which is much higher than the outdoor ROS_v of 1.1 ± 1.0 pmol m^{-3}. These values are comparable to ROS_v in urban locations of Mainz and Beijing and at a forest site in Hyytiälä, Finland (Tong et al. 2021). Indoor OP-DTT_m (41.4 ± 31.6 pmol min^{-1} μg^{-1}) is slightly higher than outdoor OP-DTT_m (26.2 ± 16.6 pmol min^{-1} μg^{-1}). As reported by Yang et al. (2024b), indoor OP-DTT_v and OP-DTT_m for background periods without activities were much lower compared to periods with activity. Note that the size fraction of outdoor PM sampled is less than 2.5 µm, whereas indoor PM ranges from 0.056 to 18 µm.

Aerosol size distribution is important to characterize for assessment of human exposure, as deposition of PM into different regions in the human respiratory tract depends strongly on particle size (Fang et al. 2019; Fang et al. 2017). Figure 2 shows distributions of (A) $EPFR_v$, (B) ROS_v, and (C) total OP-DTT_v against particle diameter (D_p) for PM collected during indoor activities of cooking, pellet burning, and mixed experiments. Among all three activities, pellet stove burning experiments show the highest $EPFR_v$ and ROS_v, while OP-DTT_v is highest for cooking activities, especially in the 10–18 µm particle diameter range. Cooking PM exhibits low values for ROS with most size ranges under the detection limit. Mixed experiments with simultaneous cooking and pellet burning exhibit intermediate values for $EPFR_v$ and ROS_v, while they show values similar to pellet burning for total OP-DTT_v. These results indicate that pellet burning shows a higher concentration of EPFRs and ROS than mixed experiments. The OP-DTT_v values for all three activities are in the similar range for submicron particles, while coarse cooking PM with D_p of 10–18 µm has a significantly high value of OP-DTT_v.

EPFRs exhibit a peak with D_p of 0.056–0.18 µm for pellet and mixed experiments as compared to coarse PM. This is likely due to higher abundance of soot or elemental carbon in the submicron range, which is known to contain EPFRs and redox-active organic compounds including polycyclic aromatic compounds and humic-like substances (HULIS) (Dou et al. 2015; Garofalo et al. 2019). Previous measurements have shown that EPFRs are mostly associated with submicron PM in urban cities in Mainz (Arangio et al. 2016) and Irvine (Fang et al. 2023), as well as in Chinese cities in Xiamen (Wang et al. 2022), Harbin (Jia et al. 2023), and Linfen (Chen et al. 2020). The main sources of EPFRs in the outdoor atmosphere are known to include vehicle tailpipe and biomass burning (Hwang et al. 2021; Fang et al. 2023). The results of this study indicate that wood burning using a pellet stove can be a significant source of EPFRs. Cooking experiments generated higher EPFRs in the coarse mode, which may be because oil-based cooking tend to generate PM with larger size (Patel et al. 2020). Other types of cooking activities such as grilling may generate higher EPFRs in submicron range, which warrants further investigations in future studies.

ROS_v for pellet burning shows a similar distribution over the entire PM diameter range, which is consistent with measurements for ambient wildfire PM (Fang et al. 2023) but is in contrast with previous measurements for urban PM which reported higher ROS from fine particles (Lu et al. 2014; Hung and Wang 2001; Kam et al. 2011). OP-DTT_v for pellet burning and mixed activities show high values in D_p of 0.056–0.18 µm and 10–18 µm. DTT-active organics, such as quinones and HULIS, generated from biomass burning are usually present in the submicron size range (Dou et al. 2015; Garofalo et al. 2019). Previous ambient measurements have shown that OP-DTT_v by

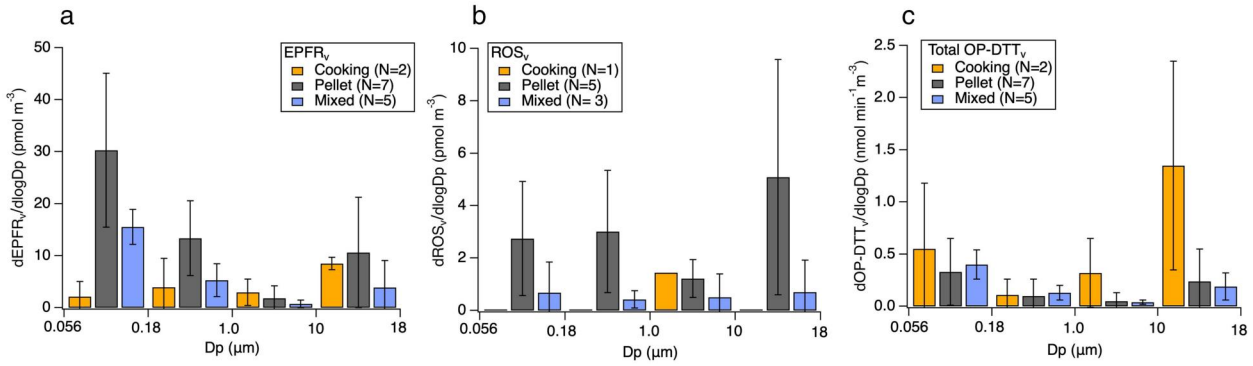

Figure 2. Size distribution of PM-volume normalized concentrations of (a) environmentally persistent free radicals ($EPFR_m$, in pmol m^{-3}) and (b) reactive oxygen species (ROS_m, in pmol m^{-3}) as well as (c) PM-mass normalized DTT activity (OP-DTT_m, in nmol min^{-1} m^{-3}) for PM emitted from indoor activities of cooking, pellet burning, and mixed experiments for simultaneous cooking and pellet burning. Error bars represent standard deviation of multiple measurements.

submicron PM is higher than coarse PM in Fresno (USA) (Charrier and Anastasio 2015) and roadside measurements in Atlanta (USA), while it is uniformly distributed for urban locations in Atlanta (Fang et al. 2017). Fang et al. (2023) showed that size distribution of OP-DTT$_v$ for wildfire PM is relatively uniform. Our results show that wood burning PM can also generate some amounts of DTT-active compounds in coarse PM (Figure 2c). Cooking activities show high OP-DTT$_v$, especially in the coarse mode, which may indicate the presence of certain DTT-active species in the coarse mode. Overall, pellet and mixed experiments show a bimodal distribution in submicron and coarse modes, while cooking experiments show higher values for coarse PM. Submicron PM is of particular concern since they can stay airborne longer with a higher likelihood of inhalation and it can penetrate deep into the respiratory system, while coarse PM deposit mostly in the upper respiratory tract (Liu et al. 2022; Lyu et al. 2017; Fang et al. 2019). Thus, the characterization of particle size-dependent health-related PM properties is crucial for a better understanding of aerosol health effects.

Correlations of EPFRs, with ROS and OP

EPFRs with semiquinone-type radical structure are redox active and form ROS in the aqueous phase (Khachatryan and Dellinger 2011; Gehling, Khachatryan, and Dellinger 2014; Valavanidis et al. 2005). EPFRs can reduce molecular oxygen to superoxide radicals, which can then be converted into H_2O_2 and to highly reactive •OH (Khachatryan et al. 2011). Thus, we assess the correlation of EPFRs with ROS formation and oxidative potential. Figure 3 shows the correlation of EPFR$_v$ with (A) ROS$_v$, (B) OP-DTT$_v$ and (C) OP-OH$_v$ for outdoor $PM_{2.5}$. We regard correlations with a coefficient of determination (R^2) <0.16 as weak, 0.16–0.49 as moderate, 0.49–0.81 as strong, and >0.81 as very strong (Schober, Boer, and Schwarte 2018). ROS$_v$ and OP-DTT$_v$ show weak correlations with EPFR$_v$ and a slightly better correlation (R^2 = 0.17) is observed for EPFR$_v$ with BMPO-OH (Figure S4). Note that EPFR$_v$ and OP-DTT$_v$ would be strongly correlated (R^2 = 0.71) if we exclude four outliers which are observed in the high pollution events as characterized by enhanced emissions from residential wood burning or vehicles (Yang et al. 2024a; Simpson et al. 2024; Edwards et al. 2024).

For indoor EPFR$_v$, we observe moderate correlations with (D) ROS$_v$ and (E) OP-DTT$_v$ with fewer number of data points. In contrast, outdoor OP-OH$_v$ shows a very strong correlation with EPFR$_v$ with R^2 = 0.83, suggesting that EPFRs are strongly related to •OH production in surrogate lung fluid. The much stronger correlation of OP-OH$_v$ measured in surrogate lung fluid compared to OH measured in water indicates the importance of lung antioxidants for redox cycling of EPFRs in generation of •OH. We could not

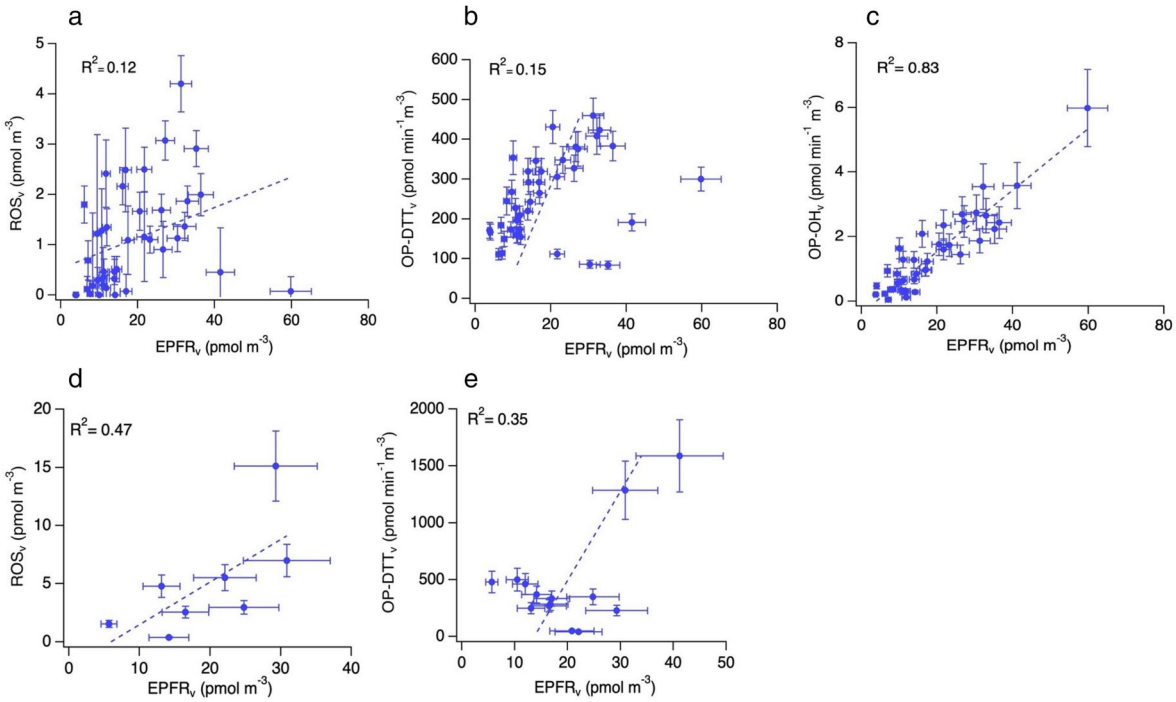

Figure 3. Correlations of outdoor EPFR$_v$ with (a) ROS$_v$, (b) OP-DTT$_v$, and (c) OP-OH$_v$ as well as of indoor EPFR$_v$ with (d) ROS$_v$ and (e) OP-DTT$_v$.

analyze OP-OH_v for indoor PM due to low mass loadings on filters, but correlations of EPFR and OP-OH should be further investigated in future studies to consolidate their relationship.

OP-DTT has been widely used as an indicator over $PM_{2.5}$ mass for assessing aerosol toxicity, with the underlying assumption that DTT decay would correspond to ROS generation. Understanding the correlations between OP-DTT and $PM_{2.5}$ mass concentrations remains important for interpreting exposure effects. $PM_{2.5}$ mass concentrations show a strong negative correlation with mass-normalized OP-DTT_m (Figure S5F), provoking the need to consider oxidative potential as a measure to understand PM health effects (Yang et al. 2024b). $EPFR_m$ also shows a negative correlation with $PM_{2.5}$ (Figure S5B), while ROS_m shows no such correlation (Figure S5D).

Figure 4 shows the correlation of outdoor ROS_v with OP-DTT_v (A) and OP-OH_v (B) as well as of indoor ROS_v with OP-DTT_v (C). No significant correlations were observed. These results are consistent with Fang et al. (2023), who also observed little correlation between ROS and OP-DTT for wildfire PM, while observing a tight correlation for traffic PM collected next to highways. Our analysis illustrates the complex relationship between ROS formation and PM oxidative potential. There are several plausible reasons for the observed low correlations. First, there may be components which are capable of forming ROS, but not active toward the DTT assay. Such compounds include organic hydroperoxides and alcohols, which can form •OH, superoxide and organic radicals *via* aqueous reactions (Wei et al. 2021a; Wei et al. 2021b). Second, our ROS measurements do not include non-radical forms of ROS such as H_2O_2 and singlet oxygen. These results encourage applications of several methods and assays for evaluating PM oxidative potential and employment of cellular assays for comprehensive evaluation of PM toxicity (Gao et al. 2020; Fang et al. 2022).

Correlations of ROS with PM components

In this section we investigate correlations of ROS and OP with PM components. Water-soluble transition metal ions including iron and copper ions are redox-active and trigger radical formation in the aqueous phase. In winter in Fairbanks, important sources of Fe and Cu are from vehicle emissions and their water-soluble fractions can also be emitted from wood burning (Yang et al. 2024a). As shown in Figure 5, water soluble (WS) fractions of iron and copper show weak to moderate positive correlations with ROS_v. The highest correlations were observed between •OH and WS-Fe ($R^2 = 0.51$, Figure 5c), followed by •OH and WS-Cu ($R^2 = 0.49$, Figure 5d). Note that WS-Cu showed a very high value for one day (1/27/2022) due to unknown reasons and was excluded from correlation analysis. These strong correlations are in line with the fact that iron and copper ions can undergo Fenton(-like) chemistry to generate •OH (Formanowicz et al. 2018; Wei et al. 2021a). Carbon-centered radicals (•R) did not show any correlations with either total or water-soluble metals. We also investigated correlations of ROS with total metal concentrations including insoluble fractions, resulting in weaker correlations (Table S2). This aligns with previous studies that have reported higher ROS correlations with soluble metal fractions (Prahalad et al. 2001; Valavanidis, Salika, and Theodoropoulou 2000; See, Wang, and Balasubramanian 2007).

Carbonaceous PM components such as elemental carbon (EC) and organic carbon (OC) may contain reactive and redox-active compounds that may generate ROS. EC is mainly emitted by vehicle tailpipe and wood burning in winter in Fairbanks. Due to limited photochemistry in winter in Fairbanks, OC is dominantly

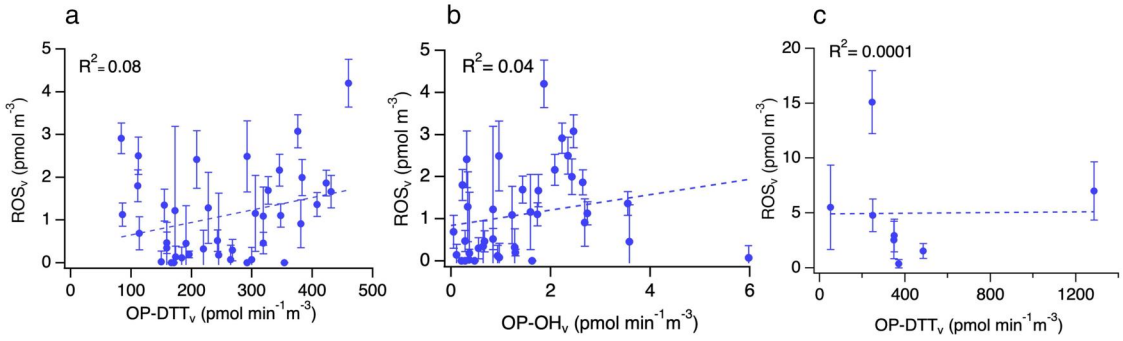

Figure 4. Correlation of ROS_v with (a) OP-DTT_v and (b) OP-OH_v for outdoor $PM_{2.5}$, and (c) correlation of ROS_v with OP-DTT_v for indoor $PM_{0.056–18}$.

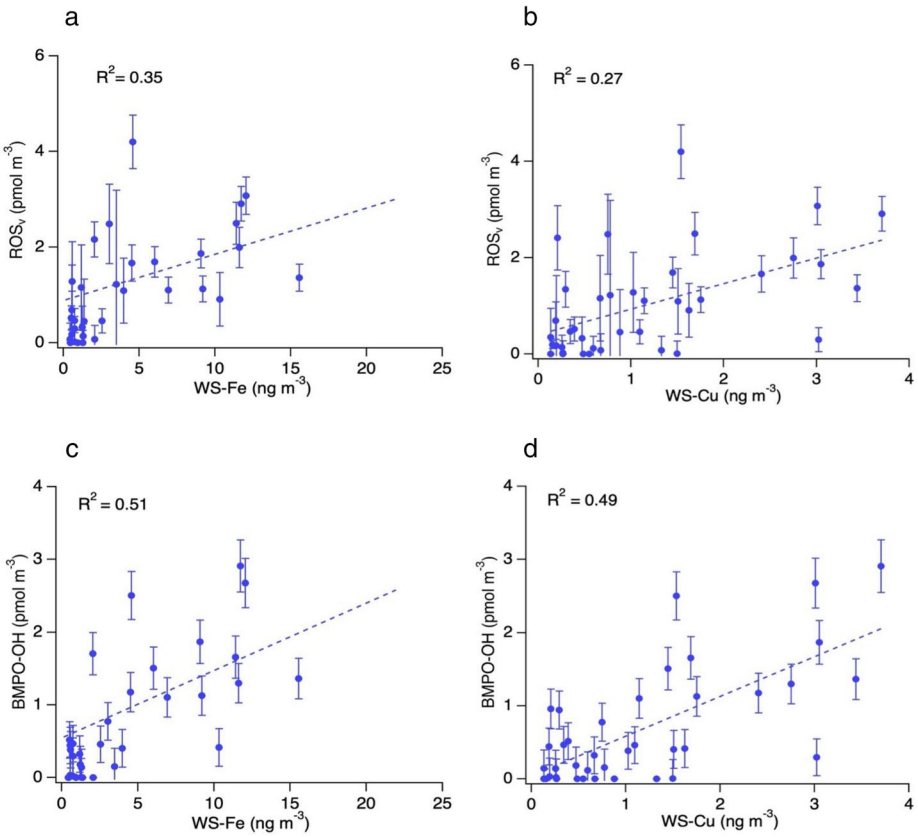

Figure 5. Correlations of ROS_v and BMPO-OH for outdoor $PM_{2.5}$ with ambient concentrations of water-soluble Fe (a and c) and water-soluble Cu (b and d). Note that one data point with anomalously high WS-Cu has been excluded from the correlation analysis.

from primary emissions, most likely from residential wood burning (Simpson et al. 2024; Yang et al. 2024a; Edwards et al. 2024). Figures 6a and b shows correlations between ambient mass concentrations of EC and OC with ROS_v and OP-DTT_v. They show moderate correlations, indicating that EC and OC play a role in ROS formation and DTT activity of PM. We also explored correlations of ROS_v with polycyclic aromatic hydrocarbons (PAHs), biomass burning organic aerosol (BBOA) and hydrocarbon-like organic aerosol (HOA), which were obtained from AMS factors. PAHs are emitted from incomplete combustion and often associated with soot or EC. BBOA are emitted by wood burning, while HOA is mostly emitted from vehicles. We observe a moderate correlation between PAHs and ROS_v, while very weak correlations are observed between ROS_v and BBOA and HOA (Figures 6c and d). These results demonstrate that ROS formation is not determined by a single component or specific source but affected by multiple components and sources. In fact, Yang et al. (2024a) applied multivariate linear regression analysis, demonstrating that the variation of OP-DTT_v can be explained by EC, BBOA, and Cu in Fairbanks.

Modeled ROS concentrations and production rates in lung fluid

We predicted the concentration (in nmol L^{-1}) of ROS in lung lining fluid using the KM-SUB-ELF model considering respiratory deposition and subsequent redox reactions of Fe, Cu, and EPFRs. The modeled ROS in lung lining fluid correlates well with WS-Fe and WS-Cu ($R^2 = 0.93$ in Figure 7a and $R^2 = 0.76$ in Figure 7b, respectively) as these transition metals participate in redox-cycling to induce ROS formation. As WS-Fe and WS-Cu are model inputs, a strong correlation is indicative that these are the main drivers of ROS formation in the model. As both correlate strongly with the modeled ROS in lung lining fluid output and, without the anomalously high WS-Cu point discussed later, WS-Cu and WS-Fe correlate strongly with each other ($R^2 = 0.61$), neither one is independently a sole predictor of ROS in lung fluid. A multilinear regression with both WS-Cu and WS-Fe as independent variables shows that approximately 92% of the variation in the model output is explained by these inputs. It should be noted that a sensitivity study reducing the WS-Fe by an order of magnitude showed a nonlinear relationship between the WS-Fe and the effect an order of magnitude

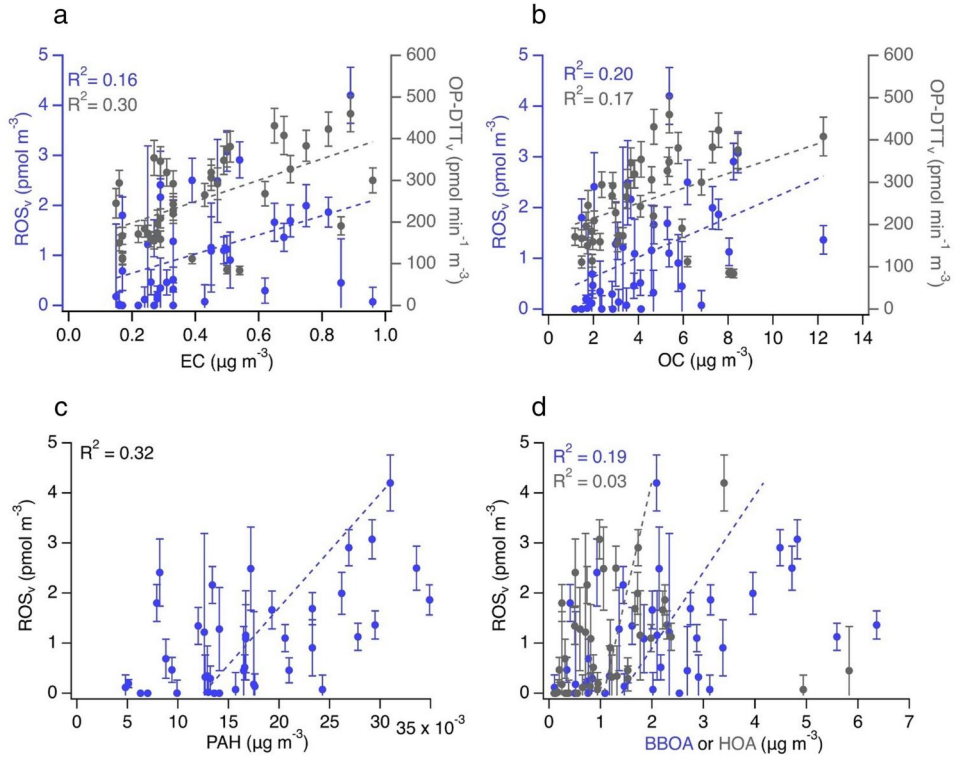

Figure 6. Correlations between ambient mass concentrations of (a) EC with ROS_v and OP-DTT_v, (b) OC with ROS_v and OP-DTT_v, (c) PAHs with ROS_v, and (d) BBOA or HOA with ROS_v.

reduction in WS-Fe had on the simulated ROS output. This result displays the model's highly nonlinear nature with complex catalytic cycling reactions where WS-Fe (and similarly WS-Cu) can both generate and destroy ROS. The correlation between modeled ROS concentration in lung fluid and $EPFR_v$ is weaker ($R^2 = 0.34$ in Figure 7c). EPFRs generate O_2^- upon reaction with molecular oxygen, which further reacts to form the more-stable H_2O_2, which can decompose to form the highly reactive OH radical. This process is also facilitated by transition metals and the weaker correlation between $EPFR_v$ and the modeled ROS in the lung may be due to the lack of correlation between $EPFR_v$ and both WS-Fe and WS-Cu ($R^2 < 0.1$ for both). While the main source of EPFR was wood burning during the campaign, the two highest $EPFR_v$ values were during the warm event (23–25 February 2022) when the main source of EPFRs was vehicle emissions with low concentrations of WS-Fe and WS-Cu (Simpson et al. 2024; Edwards et al. 2024; Yang et al. 2024a).

For the WS-Fe, $EPFR_v$, and $PM_{2.5}$ correlations with predicted ROS in lung fluid, a single measurement was removed as unrepresentative because of the high concentration of WS-Cu. Both total and water-soluble copper concentrations were unusually high on that day likely due to an unknown uncommon emission event of copper (27 January 2022). This event leads to a scenario where WS-Cu has a dominant impact on the ROS concentration in lung fluid compared to other components. To verify this, simulations were conducted where the initial concentration of each individual input component (WS-Cu, WS-Fe, $EPFR_v$, and $PM_{2.5}$) was reduced by an order of magnitude similar to an analysis done in Lakey et al. (2016). For the anomalously high WS-Cu date, the modeled ROS in lung fluid was reduced by less than 1% for an order of magnitude reduction in the initial concentration of WS-Fe or EPFRs. This indicates that WS-Cu dominated the ROS concentration, and the concentration of the other components is irrelevant for this date, justifying the removal of this point from the correlation calculation for the other three species.

Values for the simulated concentration of ROS in lung fluid are within the range of values reported in previous studies using ambient input data (Fang et al. 2019; Lakey et al. 2016). The average modeled ROS concentration in lung fluid across the data in this study is 41 nmol L^{-1}, which is comparable to values reported for small urban centers in Lakey et al. (2016). ROS in lung lining fluid exhibit a very weak correlation with a very narrow range of $PM_{2.5}$, as shown in Figure 7d. All of the data, except for the high WS-Cu point, fall below 100 nmol L^{-1}, within ROS levels characteristic of healthy individuals

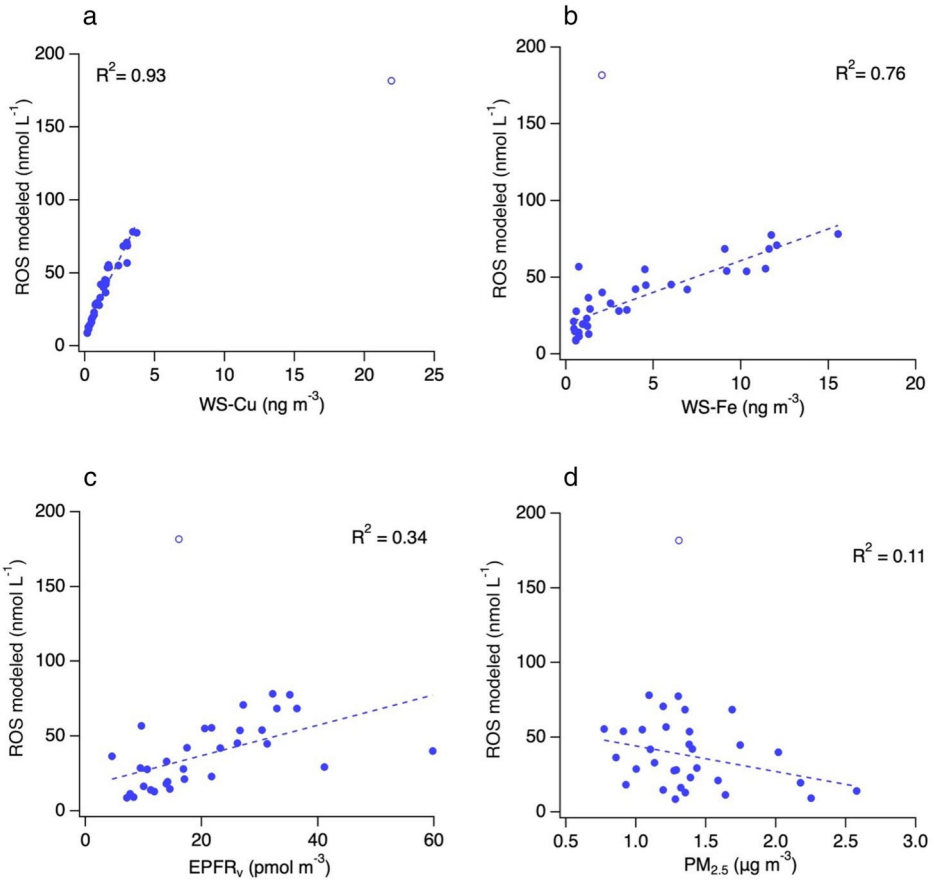

Figure 7. Correlations of simulated ROS in the lung lining fluid using KM-SUB-ELF with ambient concentrations of (a) WS-Cu, (b) WS-Fe, (c) EPFR, and (d) $PM_{2.5}$. Open circles in the plots represent data points with an anomalously high WS-Cu concentration, where concentrations of the other species are not relevant for ROS formation over the range of measurements. These points are not included in the correlation shown in the plots.

(Corradi et al. 2008; Kietzmann et al. 1993). The highest simulated concentration of ROS in lung fluid is 182 nmol L^{-1}, which is comparable to the ROS in lung fluid in Beijing and is among the highest values calculated across the approximately 50 locations investigated in Lakey et al. (2016). Note that this model only simulates ROS formation by redox reactions, but cellular ROS release by macrophages and epithelial cells would contribute significantly to total ROS in lung lining fluid (Dovrou et al. 2023; Albano et al. 2022; Fang et al. 2022).

Figure 8 shows correlations between modeled ROS production rates and OP-DTT_v. Weak correlations are seen for ROS, H_2O_2, and O_2^- family (O_2^- and its conjugate acid HO_2), but the correlation between •OH production rate and OP-DTT_v is markedly lower. This is reasonable as OP-DTT_v is known to be sensitive to Cu, which plays an important role in the formation of O_2^- and thus subsequent formation of H_2O_2 and HO_2 from O_2^-. This is supported by the strong correlation between WS-Cu and O_2^- of $R^2 = 0.78$. As the DTT assay is less sensitive to Fe, the lower correlation between OP-DTT and OH radical may be because •OH is mainly formed from Fenton reactions of H_2O_2 with Fe or other non-redox chemistry such as the decomposition of organic hydroperoxides (Tong et al. 2016; Lelieveld et al. 2021). This hypothesis is supported by the very strong correlation between WS-Fe and •OH production ($R^2 = 0.86$) and the moderate correlation between •OH production and O_2^{--} production ($R^2 = 0.34$). Removal of data points with high WS-Fe (WS-Fe > 9 ng m^{-3}), leads to higher correlations with $R^2 > 0.45$ for total ROS, the O_2^- family, and H_2O_2 production rates with DTT decay rate. These results are in better agreement with correlations found in Fang et al. (2019). The correlation between •OH production rate and OP-DTT_v remains low ($R^2 = 0.19$) even after these data points are removed.

Figure 9 shows the correlation between the simulated OH production rate in the lung fluid and $EPFR_v$. We observe a strong correlation with $R^2 = 0.67$, which is consistent with high redox activity of

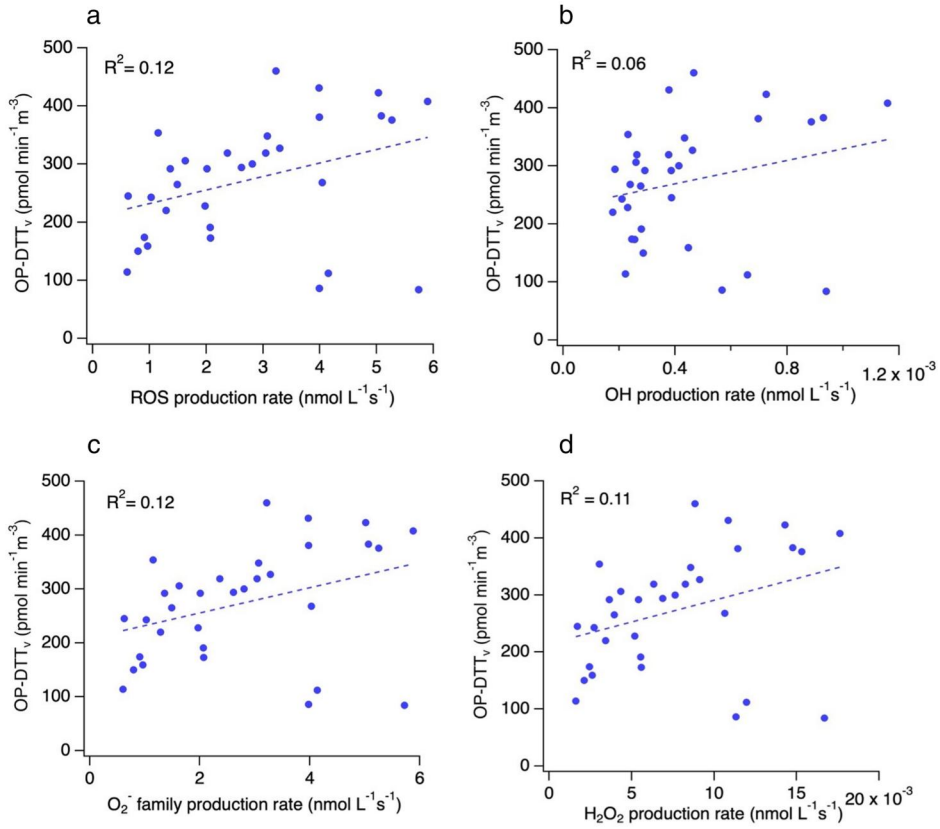

Figure 8. Correlations between OP-DTT$_v$ and simulated (a) total ROS production rate, (b) OH production rate, (c) O_2^- family production rate, and (d) H_2O_2 production rate in the lung lining fluid.

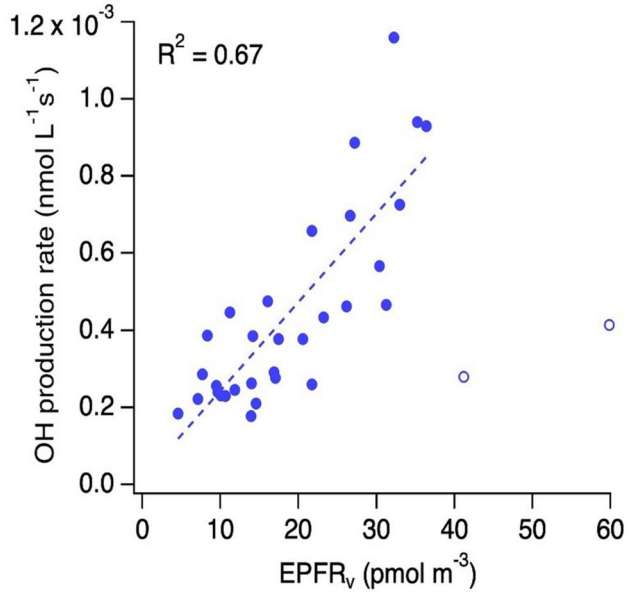

Figure 9. Correlation between the simulated OH production rate in the lung lining fluid and the measured EPFR$_v$. The open circles indicate data during a "warm event" that were removed from the correlation.

EPFRs that can form •OH *via* redox reactions (Khachatryan and Dellinger 2011; Khachatryan et al. 2011). This high correlation emerges by excluding warm events with two highest EPFR$_v$ values with lower than typical WS-Fe and WS-Cu values (marked with open circles). While the total Fe and Cu concentrations on these days is above average, due to non-tailpipe emissions, the different source may be leading to the dramatically different solubility of these metals. Interestingly, (Edwards et al. 2024) observed a very strong correlation (R^2 = 0.83) between OP-OH and EPFR$_v$ including these warm event points. As including only the water-soluble fraction of metals at these points leads to a much poorer correlation, this may indicate that under these conditions, some fraction of water-insoluble metals may participate in the formation of •OH in lung lining fluid.

Conclusions

During the ALPACA 2022 campaign, we collected outdoor and indoor PM to measure EPFRs, ROS and PM oxidative potential. We found that PM contains significant amounts of EPFRs, which is higher than previous measurements in U.S. urban cities, but lower than those in megacities in China. In indoor environments, we found that wood burning using a pellet stove is a large source of EPFRs. Upon extraction of

PM into water, we observe that both outdoor and indoor PM generates mainly hydroxyl radicals with some contribution from carbon-centered radicals. The measured values for EPFRs, ROS, and OP-DTT are similar for outdoor PM and indoor PM collected during indoor activities. For indoor PM, submicron particles generated from pellet burning showed the highest values for EPFRs, while ROS formation by PM shows little dependence on particle diameter. ROS formation in water shows little correlations with OP-DTT and OP-OH indoors or outdoors, which points toward the need for employing additional assays for OP analysis. Hydroxyl radical formation in water shows a good correlation with water soluble iron, indicating that iron released from wood burning is a likely source of hydroxyl radicals in Fairbanks. Wood burning also contributes to EC and OC, which showed moderate correlations with ROS and DTT activity of PM. We applied the KM-SUB-ELF model to estimate concentrations and production rates of ROS in lung lining fluid upon inhalation and respiratory deposition of PM. The modeled ROS concentrations in lung lining fluid are similar to those expected in small urban cities, mostly corresponding to levels characteristic of healthy individuals. Correlations of the modeled ROS production rate with OP-DTT are weak and especially low for •OH. The simulated •OH production rate in the lung fluid and $EPFR_v$ show a very strong correlation. In addition, $EPFR_v$ shows a strong positive correlation to the measured OP-OH, indicating that EPFRs undergoes redox reactions with lung antioxidants to form •OH in lung lining fluid. Our results provide useful insights on health-relevant properties of outdoor and indoor PM in cold and dark environments. These findings have important implications as they imply the need for targeted interventions in both outdoor and indoor environments and our results suggest that the reduction of residential wood burning would be beneficial to reduce human exposure to particulate matter that may cause oxidative stress and adverse health effects.

Acknowledgements

We thank the entire ALPACA science team of researchers for designing the experiment, acquiring funding, making measurements, and ongoing analysis of the results. We thank the University of Alaska Fairbanks and the Geophysical Institute for logistical support, and we thank Fairbanks for welcoming and engaging with this research. We thank Feiyang Li for support on ROS measurements.

Disclosure statement

No potential conflict of interest was reported by the author(s).

Funding

The ALPACA project was initiated as a part of PACES under IGAC and with the support of IASC. S.K., K.C.E., T.F, M.S, P.S.J.L and M.S. acknowledge funding from the U.S. National Science Foundation (AGS-1654104, CHE-2203419). W.R.S. acknowledges support from NSF grants NNA-1927750 and AGS-2109134. Y.Y. and R.J.W. were supported by the National Science Foundation's (NSF) Atmospheric Geoscience Program grant no. AGS-2029730 and the NSF Navigating the New Arctic Program grant no. NNA-1927778. E.S.R. and P.F.D. acknowledge support from the U.S. National Science Foundation's Navigating the New Arctic Program under Grants NNA-90086753 and NNA-1927750.

ORCID

Sukriti Kapur http://orcid.org/0000-0001-6645-7300
Kasey C. Edwards http://orcid.org/0009-0006-0965-8142
Ting Fang http://orcid.org/0000-0002-4845-2749
Meredith Schervish http://orcid.org/0009-0002-3365-9007
Pascale S. J. Lakey http://orcid.org/0000-0003-2923-4073
Yuhan Yang http://orcid.org/0000-0003-0343-3429
Ellis S. Robinson http://orcid.org/0000-0003-1695-6392
Peter F. DeCarlo http://orcid.org/0000-0001-6385-7149
William R. Simpson http://orcid.org/0000-0002-8596-7290
Rodney J. Weber http://orcid.org/0000-0003-0765-8035
Manabu Shiraiwa http://orcid.org/0000-0003-2532-5373

References

Ahmad, M., J. Chen, Q. Yu, M. Tariq Khan, S. Weqas Ali, A. Nawab, W. Phairuang, and S. Panyametheekul. 2023. Characteristics and Risk Assessment of Environmentally Persistent Free Radicals (EPFRs) of PM2.5 in Lahore, Pakistan. *Int. J. Environ. Res. Public Health.* 20 (3):2384. doi: 10.3390/ijerph20032384.

Albano, G. D., R. Paola Gagliardo, A. Marina Montalbano, M. Profita, G. D. Albano, R. Paola Gagliardo, A. Marina Montalbano, and M. Profita. 2022. Overview of the mechanisms of oxidative stress: impact in inflammation of the airway diseases. *Antioxidants* 11 (11):2237. doi: 10.3390/antiox11112237.

Arangio, A. M., H. Tong, J. Socorro, U. Pöschl, and M. Shiraiwa. 2016. Quantification of environmentally persistent free radicals and reactive oxygen species in atmospheric aerosol particles. *Atmos. Chem. Phys.* 16 (20):13105–19. doi: 10.5194/acp-16-13105-2016.

Birch, M. E., and R. A. Cary. 1996. Elemental carbon-based method for monitoring occupational exposures to particulate diesel exhaust. *Aerosol Sci. Technol.* 25 (3):221–41. doi: 10.1080/02786829608965393.

Borrowman, C. K., S. Zhou, T. E. Burrow, and J. P. D. Abbatt. 2016. Formation of environmentally persistent

free radicals from the heterogeneous reaction of ozone and polycyclic aromatic compounds. *Phys. Chem. Chem. Phys.* 18 (1):205–12. doi: 10.1039/C5CP05606C.

Bowling, S. A. 1979. *Air pollution in Fairbanks*. Geophysical Institute, University of Alaska Fairbanks. Accessed September 12, 2023. https://www.gi.alaska.edu/alaska-science-forum/air-pollution-fairbanks

Cesler-Maloney, M., W. R. Simpson, T. Miles, J. Mao, K. S. Law, and T. J. Roberts. 2022. Differences in ozone and particulate matter between ground level and 20 m aloft are frequent during wintertime surface-based temperature inversions in Fairbanks, Alaska. *JGR. Atmospheres* 127 (10):e2021JD036215. doi: 10.1029/2021JD036215.

Charrier, J. G., and C. Anastasio. 2012. On dithiothreitol (DTT) as a measure of oxidative potential for ambient particles: Evidence for the importance of soluble transition metals. *Atmos. Chem. Phys.* 12 (19):9321–33. doi: 10.5194/acp-12-9321-2012.

Charrier, J. G., and C. Anastasio. 2015. Rates of hydroxyl radical production from transition metals and quinones in a surrogate lung fluid. *Environ. Sci. Technol.* 49 (15): 9317–25. doi: 10.1021/acs.est.5b01606.

Chen, Q., H. Sun, W. Song, F. Cao, C. Tian, and Y.-L. Zhang. 2020. Size-resolved exposure risk of persistent free radicals (PFRs) in atmospheric aerosols and their potential sources. *Atmos. Chem. Phys.* 20 (22):14407–17. doi: 10.5194/acp-20-14407-2020.

Chen, Q., H. Sun, Z. Mu, Y. Wang, Y. Li, L. Zhang, M. Wang, and Z. Zhang. 2019. Characteristics of environmentally persistent free radicals in PM2.5: Concentrations, species and sources in Xi'an, Northwestern China. *Environ. Pollut.* 247:18–26. doi: 10.1016/j.envpol.2019.01.015.

Cho, A. K., C. Sioutas, A. H. Miguel, Y. Kumagai, D. A. Schmitz, M. Singh, A. Eiguren-Fernandez, and J. R. Froines. 2005. Redox activity of airborne particulate matter at different sites in the Los Angeles Basin. *Environ. Res.* 99 (1):40–7. doi: 10.1016/j.envres.2005.01.003.

Corradi, M., P. Pignatti, G. Brunetti, M. Goldoni, A. Caglieri, S. Nava, G. Moscato, and B. Balbi. 2008. Comparison between exhaled and bronchoalveolar lavage levels of hydrogen peroxide in patients with diffuse interstitial lung diseases. *Acta Biomed.* 79 (Suppl 1):73–8. http://europepmc.org/abstract/MED/18924312.

Daellenbach, K. R., G. Uzu, J. Jiang, L.-E. Cassagnes, Z. Leni, A. Vlachou, G. Stefenelli, F. Canonaco, S. Weber, A. Segers, et al. 2020. Sources of particulate-matter air pollution and its oxidative potential in Europe. *Nature* 587 (7834):414–9. doi: 10.1038/s41586-020-2902-8.

Dellinger, B., S. Lomnicki, L. Khachatryan, Z. Maskos, R. W. Hall, J. Adounkpe, C. McFerrin, and H. Truong. 2007. Formation and stabilization of persistent free radicals. *Proc. Combust. Inst.* 31 (1):521–8. doi: 10.1016/j.proci.2006.07.172.

Dellinger, B., W. A. Pryor, B. Cueto, G. L. Squadrito, and W. A. Deutsch. 2000. The role of combustion-generated radicals in the toxicity of PM2.5. *Proc. Combust. Inst.* 28 (2):2675–81. doi: 10.1016/S0082-0784(00)80687-6.

Dou, J., P. Lin, B.-Y. Kuang, and J. Z. Yu. 2015. Reactive oxygen species production mediated by humic-like substances in atmospheric aerosols: Enhancement effects by pyridine, imidazole, and their derivatives. *Environ. Sci. Technol.* 49 (11):6457–65. doi: 10.1021/es5059378.

Dovrou, E., S. Lelieveld, A. Mishra, U. Pöschl, and T. Berkemeier. 2023. Influence of ambient and endogenous H_2O_2 on reactive oxygen species concentrations and OH radical production in the respiratory tract. *Environ. Sci. Atmos.* 3 (7):1066–74. doi: 10.1039/D2EA00179A.

Edwards, K. C., A. L. Klodt, T. Galeazzo, M. Schervish, J. Wei, T. Fang, N. M. Donahue, B. Aumont, S. A. Nizkorodov, and M. Shiraiwa. 2022. Effects of nitrogen oxides on the production of reactive oxygen species and environmentally persistent free radicals from α-pinene and naphthalene secondary organic aerosols. *J. Phys. Chem. A* 126 (40):7361–72. doi: 10.1021/acs.jpca.2c05532.

Edwards, K. C., S. Kapur, T. Fang, M. Cesler-Maloney, Y. Yang, A. L. Holen, J. Wu, E. S. Robinson, P. F. Decarlo, K. A. Pratt, et al. 2024. Residential wood burning and vehicle emissions as major sources of environmentally persistent free radicals in Fairbanks, Alaska. *Environ. Sci. Technol.* 58 (32):14293–305. doi: 10.1021/acs.est.4c01206.

Fang, T., B. C. H. Hwang, S. Kapur, K. S. Hopstock, J. Wei, V. Nguyen, S. A. Nizkorodov, and M. Shiraiwa. 2023. Wildfire particulate matter as a source of environmentally persistent free radicals and reactive oxygen species. *Environ. Sci: Atmos.* 3 (3):581–94. doi: 10.1039/D2EA00170E.

Fang, T., L. Zeng, D. Gao, V. Verma, A. B. Stefaniak, and R. J. Weber. 2017. Ambient size distributions and lung deposition of aerosol dithiothreitol-measured oxidative potential: Contrast between soluble and insoluble particles. *Environ. Sci. Technol.* 51 (12):6802–11. doi: 10.1021/acs.est.7b01536.

Fang, T., P. S. J. Lakey, R. J. Weber, and M. Shiraiwa. 2019. Oxidative potential of particulate matter and generation of reactive oxygen species in epithelial lining fluid. *Environ. Sci. Technol.* 53 (21):12784–92. doi: 10.1021/acs.est.9b03823.

Fang, T., V. Verma, H. Guo, L. E. King, E. S. Edgerton, and R. J. Weber. 2015. A semi-automated system for quantifying the oxidative potential of ambient particles in aqueous extracts using the dithiothreitol (DTT) assay: Results from the Southeastern Center for Air Pollution and Epidemiology (SCAPE). *Atmos. Meas. Tech.* 8 (1):471–82. doi: 10.5194/amt-8-471-2015.

Fang, T., V. Verma, J. T. Bates, J. Abrams, M. Klein, M. J. Strickland, S. E. Sarnat, H. H. Chang, J. A. Mulholland, P. E. Tolbert, et al. 2016. Oxidative potential of ambient water-soluble PM2.5 in the southeastern United States: Contrasts in sources and health associations between ascorbic acid (AA) and dithiothreitol (DTT) assays. *Atmos. Chem. Phys.* 16 (6):3865–79. doi: 10.5194/acp-16-3865-2016.

Fang, T., Y.-K. Huang, J. Wei, J. E. Monterrosa Mena, P. S. J. Lakey, M. T. Kleinman, M. A. Digman, and M. Shiraiwa. 2022. Superoxide release by macrophages through NADPH oxidase activation dominating chemistry by isoprene secondary organic aerosols and quinones to cause oxidative damage on membranes. *Environ. Sci. Technol.* 56 (23):17029–38. doi: 10.1021/acs.est.2c03987.

Finkel, T., and N. J. Holbrook. 2000. Oxidants, oxidative stress and the biology of ageing. *Nature* 408 (6809):239–47. doi: 10.1038/35041687.

Fochesatto, G. J., J. A. Mayfield, D. P. Starkenburg, M. A. Gruber, and J. Conner. 2015. Occurrence of shallow cold

flows in the winter atmospheric boundary layer of interior of Alaska. *Meteorol. Atmos. Phys.* 127 (4):369–82. doi: 10.1007/s00703-013-0274-4.

Formanowicz, D., M. Radom, A. Rybarczyk, and P. Formanowicz. 2018. The role of Fenton reaction in ROS-induced toxicity underlying atherosclerosis – modeled and analyzed using a Petri net-based approach. *Biosystems.* 165:71–87. doi: 10.1016/j.biosystems.2018.01.002.

Gao, D., S. Ripley, S. Weichenthal, and K. J. Godri Pollitt. 2020. Ambient particulate matter oxidative potential: Chemical determinants, associated health effects, and strategies for risk management. *Free Radic. Biol. Med.* 151:7–25. doi: 10.1016/j.freeradbiomed.2020.04.028.

Gao, D., T. Fang, V. Verma, L. G. Zeng, and R. J. Weber. 2017. A method for measuring total aerosol oxidative potential (OP) with the dithiothreitol (DTT) assay and comparisons between an urban and roadside site of water-soluble and total OP. *Atmos. Meas. Tech.* 10 (8): 2821–35. doi: 10.5194/amt-10-2821-2017.

Garofalo, L. A., M. A. Pothier, E. J. T. Levin, T. Campos, S. M. Kreidenweis, and D. K. Farmer. 2019. Emission and evolution of submicron organic aerosol in smoke from wildfires in the western United States. *ACS Earth Space Chem.* 3 (7):1237–47. doi: 10.1021/acsearthspacechem.9b00125.

Gehling, W., and B. Dellinger. 2013. Environmentally persistent free radicals and their lifetimes in PM2.5. *Environ. Sci. Technol.* 47 (15):8172–8. doi: 10.1021/es401767m.

Gehling, W., L. Khachatryan, and B. Dellinger. 2014. Hydroxyl radical generation from environmentally persistent free radicals (EPFRs) in $PM_{2.5}$. *Environ. Sci. Technol.* 48 (8):4266–72. doi: 10.1021/es401770y.

Hung, H.-F., and C.-S. Wang. 2001. Experimental determination of reactive oxygen species in Taipei aerosols. *J. Aerosol Sci.* 32 (10):1201–11. doi: 10.1016/S0021-8502(01)00051-9.

Hwang, B., T. Fang, R. Pham, J. Wei, S. Gronstal, B. Lopez, C. Frederickson, T. Galeazzo, X. Wang, H. Jung, et al. 2021. Environmentally persistent free radicals, reactive oxygen species generation, and oxidative potential of highway PM2.5. *ACS Earth Space Chem.* 5 (8):1865–75. doi: 10.1021/acsearthspacechem.1c00135.

Jia, H., S. Li, L. Wu, S. Li, V. K. Sharma, and B. Yan. 2020. Cytotoxic free radicals on air-borne soot particles generated by burning wood or low-maturity coals. *Environ. Sci. Technol.* 54 (9):5608–18. doi: 10.1021/acs.est.9b06395.

Jia, S.-M., D.-Q. Wang, L.-Y. Liu, Z.-F. Zhang, and W.-L. Ma. 2023. Size-resolved environmentally persistent free radicals in cold region atmosphere: Implications for inhalation exposure risk. *J. Hazard. Mater.* 443 (Pt B): 130263. doi: 10.1016/j.jhazmat.2022.130263.

Jiang, H., C. M. S. Ahmed, A. Canchola, J. Y. Chen, and Y.-H. Lin. 2019. Use of dithiothreitol assay to evaluate the oxidative potential of atmospheric aerosols. *Atmosphere* 10 (10):571. doi: 10.3390/atmos10100571.

Joyce, P. L., R. Von Glasow, and W. R. Simpson. 2014. The fate of NOx emissions due to nocturnal oxidation at high latitudes: 1-D simulations and sensitivity experiments. *Atmos. Chem. Phys.* 14 (14):7601–16. doi: 10.5194/acp-14-7601-2014.

Kam, W., Z. Ning, M. M. Shafer, J. J. Schauer, and C. Sioutas. 2011. Chemical characterization and redox potential of coarse and fine particulate matter (PM) in underground and ground-level rail systems of the Los Angeles Metro. *Environ. Sci. Technol.* 45 (16):6769–76. doi: 10.1021/es201195e.

Khachatryan, L., and B. Dellinger. 2011. Environmentally persistent free radicals (EPFRs)-2. Are free hydroxyl radicals generated in aqueous solutions? *Environ. Sci. Technol.* 45 (21):9232–9. doi: 10.1021/es201702q.

Khachatryan, L., E. Vejerano, S. Lomnicki, and B. Dellinger. 2011. Environmentally persistent free radicals (EPFRs). 1. Generation of reactive oxygen species in aqueous solutions. *Environ. Sci. Technol.* 45 (19):8559–66. doi: 10.1021/es201309c.

Kietzmann, D., R. Kahl, M. Müller, H. Burchardi, D. Kettler, D. Kietzmann, R. Kahl, M. Müller, H. Burchardi, and D. Kettler. 1993. Hydrogen peroxide in expired breath condensate of patients with acute respiratory failure and with ARDS. *Intensive Care Med.* 19 (2) (2):78–81. doi: 10.1007/BF01708366.

Kotchenruther, R. A. 2016. Source apportionment of PM2.5 at multiple Northwest US sites: Assessing regional winter wood smoke impacts from residential wood combustion. *Atmos. Environ.* 142:210–9. doi: 10.1016/j.atmosenv.2016.07.048.

Kumagai, Y., S. Koide, K. Taguchi, A. Endo, Y. Nakai, T. Yoshikawa, and N. Shimojo. 2002. Oxidation of proximal protein sulfhydryls by phenanthraquinone, a component of diesel exhaust particles. *Chem. Res. Toxicol.* 15 (4): 483–9. doi: 10.1021/tx0100993.

Lakey, P. S. J., T. Berkemeier, H. Tong, A. M. Arangio, K. Lucas, U. Pöschl, and M. Shiraiwa. 2016. Chemical exposure-response relationship between air pollutants and reactive oxygen species in the human respiratory tract. *Sci. Rep.* 6 (1):32916. doi: 10.1038/srep32916.

Lelieveld, S., J. Wilson, E. Dovrou, A. Mishra, P. S. J. Lakey, M. Shiraiwa, U. Pöschl, and T. Berkemeier. 2021. Hydroxyl radical production by air pollutants in epithelial lining fluid governed by interconversion and scavenging of reactive oxygen species. *Environ. Sci. Technol.* 55 (20): 14069–79. doi: 10.1021/acs.est.1c03875.

Liu, W., W. Du, J. Wang, S. Zhuo, Y. Chen, N. Lin, G. Kong, and B. Pan. 2022. PAHs bound to submicron particles in rural Chinese homes burning solid fuels. *Ecotoxicol. Environ. Saf.* 247:114274. doi: 10.1016/j.ecoenv.2022.114274.

Lu, S., F. Yi, X. Hao, S. Yu, J. Ren, M. Wu, F. Jialiang, S. Yonemochi, and Q. Wang. 2014. Physicochemical properties and ability to generate free radicals of ambient coarse, fine, and ultrafine particles in the atmosphere of Xuanwei, China, an area of high lung cancer incidence. *Atmos. Environ.* 97:519–28. doi: 10.1016/j.atmosenv.2013.11.047.

Lyu, Y., K. Zhang, F. Chai, T. Cheng, Q. Yang, Z. Zheng, and X. Li. 2017. Atmospheric size-resolved trace elements in a city affected by non-ferrous metal smelting: Indications of respiratory deposition and health risk. *Environ. Pollut.* 224: 559–71. doi: 10.1016/j.envpol.2017.02.039.

Marelle, L., J. C. Raut, K. S. Law, and O. Duclaux. 2018. Current and future arctic aerosols and ozone from remote emissions and emerging local sources-modeled source contributions and radiative effects. *J. Geophys. Res.-Atmos.* 123 (22):12942–63. doi: 10.1029/2018jd028863.

Oeder, S., S. Dietrich, I. Weichenmeier, W. Schober, G. Pusch, R. A. Jörres, R. Schierl, D. Nowak, H. Fromme, H. Behrendt, et al. 2012. Toxicity and elemental composition of particulate matter from outdoor and indoor air of elementary schools in Munich, Germany. *Indoor Air.* 22 (2):148–58. doi: 10.1111/j.1600-0668.2011.00743.x.

Patel, S., S. Sankhyan, E. K. Boedicker, P. F. DeCarlo, D. K. Farmer, A. H. Goldstein, E. F. Katz, W. W. Nazaroff, Y. Tian, J. Vanhanen, et al. 2020. Indoor particulate matter during HOMEChem: Concentrations, size distributions, and exposures. *Environ. Sci. Technol.* 54 (12):7107–16. doi: 10.1021/acs.est.0c00740.

Pöschl, U., and M. Shiraiwa. 2015. Multiphase chemistry at the atmosphere–Biosphere interface influencing climate and public health in the anthropocene. *Chem. Rev.* 115 (10):4440–75. doi: 10.1021/cr500487s.

Prahalad, A. K., J. Inmon, L. A. Dailey, M. C. Madden, A. J. Ghio, and J. E. Gallagher. 2001. Air pollution particles mediated oxidative dna base damage in a cell free system and in human airway epithelial cells in relation to particulate metal content and bioreactivity. *Chem. Res. Toxicol.* 14 (7):879–87. doi: 10.1021/tx010022e.

Ripley, S., D. Gao, K. J. G. Pollitt, P. S. J. Lakey, M. Shiraiwa, M. Hatzopoulou, and S. Weichenthal. 2023. Within-city spatial variations in long-term average outdoor oxidant gas concentrations and cardiovascular mortality: Effect modification by oxidative potential in the Canadian Census Health and Environment Cohort. *Environ. Epidemiol.* 7 (4):e257. doi: 10.1097/EE9.0000000000000257.

Robinson, E. S., M. Cesler-Maloney, X. Tan, J. Mao, W. Simpson, and P. F. Decarlo. 2023. Wintertime spatial patterns of particulate matter in Fairbanks, AK during ALPACA 2022. *Environ. Sci. Atmos.* 3 (3):568–80. doi: 10.1039/D2EA00140C.

Runberg, H. L., D. G. Mitchell, S. S. Eaton, G. R. Eaton, and B. J. Majestic. 2020. Stability of environmentally persistent free radicals (EPFR) in atmospheric particulate matter and combustion particles. *Atmos. Environ.* 240: 117809. doi: 10.1016/j.atmosenv.2020.117809.

Salana, S., H. Yu, Z. Dai, P. S. G. Subramanian, J. V. Puthussery, Y. Wang, A. Singh, F. D. Pope, M. A. Leiva G, N. Rastogi, et al. 2024. Inter-continental variability in the relationship of oxidative potential and cytotoxicity with PM2.5 mass. *Nat. Commun.* 15 (1):5263. doi: 10.1038/s41467-024-49649-4.

Schober, P., C. Boer, and L. A. Schwarte. 2018. Correlation coefficients: Appropriate use and interpretation. *Anesth. Analg.* 126 (5):1763–8. doi: 10.1213/ANE.0000000000002864.

See, S. W., Y. H. Wang, and R. Balasubramanian. 2007. Contrasting reactive oxygen species and transition metal concentrations in combustion aerosols. *Environ. Res.* 103 (3):317–24. doi: 10.1016/j.envres.2006.08.012.

Shahpoury, P., Z. W. Zhang, A. Filippi, S. Hildmann, S. Lelieveld, B. Mashtakov, B. R. Patel, A. Traub, D. Umbrio, M. Wietzoreck, et al. 2022. Inter-comparison of oxidative potential metrics for airborne particles identifies differences between acellular chemical assays. *Atmos. Pollut. Res.* 13 (12):101596. doi: 10.1016/j.apr.2022.101596.

Shen, J., S. Taghvaee, C. La, F. Oroumiyeh, J. Liu, M. Jerrett, S. Weichenthal, I. Del Rosario, M. M. Shafer, B. Ritz, et al. 2022. Aerosol oxidative potential in the greater Los Angeles area: Source apportionment and associations with socioeconomic position. *Environ. Sci. Technol.* 56 (24):17795–804. doi: 10.1021/acs.est.2c02788.

Shiraiwa, M., K. Ueda, G. Andrea Pozzer, C. J. Lammel, A. Kampf, S. Fushimi, A. M. Enami, J. Arangio, Y. Fröhlich-Nowoisky, A. Fujitani, et al. 2017. Aerosol health effects from molecular to global scales. *Environ. Sci. Technol.* 51 (23):13545–67. doi: 10.1021/acs.est.7b04417.

Sies, H., C. Berndt, and D. P. Jones. 2017. Oxidative stress. *Annu. Rev. Biochem.* 86 (1):715–48. doi: 10.1146/annurev-biochem-061516-045037.

Simpson, W. R., J. Mao, G. J. Fochesatto, K. S. Law, P. F. DeCarlo, J. Schmale, K. A. Pratt, S. R. Arnold, J. Stutz, J. E. Dibb, et al. 2024. Overview of the Alaskan layered pollution and chemical analysis (ALPACA) field experiment. *ACS EST. Air.* 1 (3):200–22. doi: 10.1021/acsestair.3c00076.

Son, Y., V. Mishin, W. Welsh, S.-E. Lu, J. Laskin, H. Kipen, and Q. Meng. 2015. A novel high-throughput approach to measure hydroxyl radicals induced by airborne particulate matter. *Int. J. Environ. Res. Public Health.* 12 (11):13678–95. doi: 10.3390/ijerph121113678.

Squadrito, G. L., R. Cueto, B. Dellinger, and W. A. Pryor. 2001. Quinoid redox cycling as a mechanism for sustained free radical generation by inhaled airborne particulate matter. *Free Radic. Biol. Med.* 31 (9):1132–8. doi: 10.1016/S0891-5849(01)00703-1.

Stieb, D. M., G. J. Evans, T. M. To, P. S. J. Lakey, M. Shiraiwa, M. Hatzopoulou, L. Minet, J. R. Brook, R. T. Burnett, and S. A. Weichenthal. 2021. Within-city variation in reactive oxygen species from fine particle air pollution and COVID-19. *Am. J. Respir. Crit. Care Med.* 204 (2):168–77. doi: 10.1164/rccm.202011-4142OC.

Thomas, M. A., A. Devasthale, M. Tjernström, and A. M. L. Ekman. 2019. The Relation Between Aerosol Vertical Distribution and Temperature Inversions in the Arctic in Winter and Spring. *Geophys. Res. Lett.* 46 (5):2836–45. doi: 10.1029/2018GL081624.

Tong, H., A. M. Arangio, P. S. J. Lakey, T. Berkemeier, F. Liu, C. J. Kampf, W. H. Brune, U. Pöschl, and M. Shiraiwa. 2016. Hydroxyl radicals from secondary organic aerosol decomposition in water. *Atmos. Chem. Phys.* 16 (3):1761–71. doi: 10.5194/acp-16-1761-2016.

Tong, H., F. Liu, A. Filippi, J. Wilson, A. M. Arangio, Y. Zhang, S. Yue, S. Lelieveld, F. Shen, H.-M. K. Keskinen, et al. 2021. Aqueous-phase reactive species formed by fine particulate matter from remote forests and polluted urban air. *Atmos. Chem. Phys.* 21 (13):10439–55. doi: 10.5194/acp-21-10439-2021.

Tong, H., P. S. J. Lakey, A. M. Arangio, J. Socorro, F. Shen, K. Lucas, W. H. Brune, U. Pöschl, and M. Shiraiwa. 2018. Reactive oxygen species formed by secondary organic aerosols in water and surrogate lung fluid. *Environ. Sci. Technol.* 52 (20):11642–51. doi: 10.1021/acs.est.8b03695.

United States Environmental Protection Agency. n.d. "Indoor Air Quality and Climate Change." EPA. Accessed September 8, 2023. https://www.epa.gov/indoor-air-quality-iaq/indoor-air-quality-and-climate-change

United States Environmental Protection Agency. 2014. *Method 6020B (SW-846): inductively coupled plasma*. Washington, DC: Mass Spectrometry.

Valavanidis, A., A. Salika, and A. Theodoropoulou. 2000. Generation of hydroxyl radicals by urban suspended particulate air matter. The role of iron ions. *Atmospheric Environment* 34 (15):2379–86. doi: 10.1016/S1352-2310(99)00435-5.

Valavanidis, A., K. Fiotakis, E. Bakeas, and T. Vlahogianni. 2005. Electron paramagnetic resonance study of the generation of reactive oxygen species catalysed by transition metals and quinoid redox cycling by inhalable ambient particulate matter. *Redox Rep.* 10 (1):37–51. doi: 10.1179/135100005x21606.

Verma, V., Y. Wang, R. El-Afifi, T. Fang, J. Rowland, A. G. Russell, and R. J. Weber. 2015. Fractionating ambient humic-like substances (HULIS) for their reactive oxygen species activity - Assessing the importance of quinones and atmospheric aging. *Atmos. Environ.* 120:351–9. doi: 10.1016/j.atmosenv.2015.09.010.

Vicente, E. D., A. M. Vicente, M. Evtyugina, F. I. Oduber, F. Amato, X. Querol, and C. Alves. 2020. Impact of wood combustion on indoor air quality. *Sci. Total Environ.* 705: 135769. doi: 10.1016/j.scitotenv.2019.135769.

Vidrio, E., H. Jung, and C. Anastasio. 2008. Generation of hydroxyl radicals from dissolved transition metals in surrogate lung fluid solutions. *Atmos. Environ.* 42 (18):4369–79. doi: 10.1016/j.atmosenv.2008.01.004.

Wang, Y., K. Yao, X. Fu, X. Zhai, L. Jin, and H. Guo. 2022. Size-resolved exposure risk and subsequent role of environmentally persistent free radicals (EPFRs) from atmospheric particles. *Atmos. Environ.* 276:119059. doi: 10.1016/j.atmosenv.2022.119059.

Ward, T., B. Trost, J. Conner, J. Flanagan, and R. K. M. Jayanty. 2012. Source apportionment of PM2.5 in a subarctic airshed – Fairbanks, Alaska. *Aerosol Air Qual. Res.* 12 (4):536–43. doi: 10.4209/aaqr.2011.11.0208.

Wei, J., T. Fang, C. Wong, P. S. J. Lakey, S. A. Nizkorodov, and M. Shiraiwa. 2021b. Superoxide formation from aqueous reactions of biogenic secondary organic aerosols. *Environ. Sci. Technol.* 55 (1):260–70. doi: 10.1021/acs.est.0c07789.

Wei, J., T. Fang, P. S. J. Lakey, and M. Shiraiwa. 2021a. Iron-facilitated organic radical formation from secondary organic aerosols in surrogate lung fluid. *Environ. Sci. Technol.* 56 (11):7234–7243. doi: 10.1021/acs.est.1c04334.

Wendler, G., and M. Shulski. 2009. A century of climate change for Fairbanks, Alaska. *Arctic* 62 (3):295–300. doi: 10.14430/arctic149.

Win, M. S., Z. Y. Tian, H. Zhao, K. Xiao, J. X. Peng, Y. Shang, M. H. Wu, G. L. Xiu, S. L. Lu, S. Yonemochi, et al. 2018. Atmospheric HULIS and its ability to mediate the reactive oxygen species (ROS): A review. *J. Environ. Sci.* 71:13–31. doi: 10.1016/j.jes.2017.12.004.

Xiong, Q., H. Yu, R. Wang, J. Wei, and V. Verma. 2017. Rethinking dithiothreitol-based particulate matter oxidative potential: Measuring dithiothreitol consumption versus reactive oxygen species generation. *Environ. Sci. Technol.* 51 (11):6507–14. doi: 10.1021/acs.est.7b01272.

Yang, L., G. Liu, M. Zheng, R. Jin, Q. Zhu, Y. Zhao, X. Wu, and Y. Xu. 2017. Highly elevated levels and particle-size distributions of environmentally persistent free radicals in haze-associated atmosphere. *Environ. Sci. Technol.* 51 (14):7936–44. doi: 10.1021/acs.est.7b01929.

Yang, Y., D. Gao, and R. J. Weber. 2021. A method for liquid spectrophotometric measurement of total and water-soluble iron and copper in ambient aerosols. *Atmos. Meas. Tech.* 14 (6):4707–19. doi: 10.5194/amt-14-4707-2021.

Yang, Y., M. A. Battaglia, E. S. Robinson, P. F. DeCarlo, K. C. Edwards, T. Fang, S. Kapur, M. Shiraiwa, M. Cesler-Maloney, W. R. Simpson, et al. 2024b. Indoor–Outdoor Oxidative Potential of PM2.5 in Wintertime Fairbanks. Alaska: Impact of Air Infiltration and Indoor Activities." ACS ES&T Air. doi: 10.1021/acsestair.3c00067.

Yang, Y., M. A. Battaglia, M. K. Mohan, E. S. Robinson, P. F. Decarlo, K. C. Edwards, T. Fang, S. Kapur, M. Shiraiwa, M. Cesler-Maloney, et al. 2024a. Assessing the oxidative potential of outdoor $PM_{2.5}$ in wintertime Fairbanks, Alaska. *ACS EST. Air.* 1 (3):175–87. doi: 10.1021/acsestair.3c00066.

Yu, H., J. Varghese Puthussery, Y. Wang, and V. Verma. 2021. Spatiotemporal variability in the oxidative potential of ambient fine particulate matter in the Midwestern United States. *Atmos. Chem. Phys.* 21 (21):16363–86. doi: 10.5194/acp-21-16363-2021.